Gaia Data Release 2: Kinematics of globular clusters and dwarf galaxies around the Milky Way

A&A 616, A12 (2018)
https://doi.org/10.1051/0004-6361/201832698

Astronomy & Astrophysics

Special issue

Gaia Data Release 2

Gaia Data Release 2

Kinematics of globular clusters and dwarf galaxies around the Milky Way⋆

Gaia Collaboration, A. Helmi[1,⋆⋆], F. van Leeuwen[2], P. J. McMillan[3], D. Massari[1], T. Antoja[4,5], A. C. Robin[6], L. Lindegren[3], U. Bastian[7], F. Arenou[8], C. Babusiaux[8,9], M. Biermann[7], M. A. Breddels[1], D. Hobbs[3], C. Jordi[5], E. Pancino[10,11], C. Reylé[6], J. Veljanoski[1], A. G. A. Brown[12], A. Vallenari[13], T. Prusti[4], J. H. J. de Bruijne[4], C. A. L. Bailer-Jones[14], D. W. Evans[2], L. Eyer[15], F. Jansen[16], S. A. Klioner[17], U. Lammers[18], X. Luri[5], F. Mignard [19], C. Panem[20], D. Pourbaix[21,22], S. Randich[10], P. Sartoretti[8], H. I. Siddiqui[23], C. Soubiran[24], N. A. Walton[2], M. Cropper[25], R. Drimmel[26], D. Katz[8], M. G. Lattanzi[26], J. Bakker[18], C. Cacciari[27], J. Castañeda[5], L. Chaoul[20], N. Cheek[28], F. De Angeli[2], C. Fabricius[5], R. Guerra[18], B. Holl[15], E. Masana[5], R. Messineo[29], N. Mowlavi[15], K. Nienartowicz[30], P. Panuzzo[8], J. Portell[5], M. Riello[2], G. M. Seabroke[25], P. Tanga[19], F. Thévenin[19], G. Gracia-Abril[31,7], G. Comoretto[23], M. Garcia-Reinaldos[18], D. Teyssier[23], M. Altmann[7,32], R. Andrae[14], M. Audard[15], I. Bellas-Velidis[33], K. Benson[25], J. Berthier[34], R. Blomme[35], P. Burgess[2], G. Busso[2], B. Carry[19,34], A. Cellino[26], G. Clementini[27], M. Clotet[5], O. Creevey[19,36], M. Davidson[37], J. De Ridder[38], L. Delchambre[39], A. Dell'Oro[10], C. Ducourant[24], J. Fernández-Hernández[40], M. Fouesneau[14], Y. Frémat[35], L. Galluccio[19], M. García-Torres[41], J. González-Núñez[28,42], J. J. González-Vidal[5], E. Gosset[39,22], L. P. Guy[30,43], J.-L. Halbwachs[44], N. C. Hambly[37], D. L. Harrison[2,45], J. Hernández[18], D. Hestroffer[34], S. T. Hodgkin[2], A. Hutton[46], G. Jasniewicz[47], A. Jean-Antoine-Piccolo[20], S. Jordan[7], A. J. Korn[48], A. Krone-Martins[49], A. C. Lanzafame[50,51], T. Lebzelter[52], W. Löffler[7], M. Manteiga[53,54], P. M. Marrese[55,11], J. M. Martín-Fleitas[46], A. Moitinho[49], A. Mora[46], K. Muinonen[56,57], J. Osinde[58], T. Pauwels[35], J.-M. Petit[6], A. Recio-Blanco[19], P. J. Richards[59], L. Rimoldini[30], L. M. Sarro[60], C. Siopis[21], M. Smith[25], A. Sozzetti[26], M. Süveges[14], J. Torra[5], W. van Reeven[46], U. Abbas[26], A. Abreu Aramburu[61], S. Accart[62], C. Aerts[38,63], G. Altavilla[55,11,27], M. A. Álvarez[53], R. Alvarez[18], J. Alves[52], R. I. Anderson[64,15], A. H. Andrei[65,66,32], E. Anglada Varela[40], E. Antiche[5], B. Arcay[53], T. L. Astraatmadja[14,67], N. Bach[46], S. G. Baker[25], L. Balaguer-Núñez[5], P. Balm[23], C. Barache[32], C. Barata[49], D. Barbato[68,26], F. Barblan[15], P. S. Barklem[48], D. Barrado[69], M. Barros[49], M. A. Barstow[70], S. Bartholomé Muñoz[5], J.-L. Bassilana[62], U. Becciani[51], M. Bellazzini[27], A. Berihuete[71], S. Bertone[26,32,72], L. Bianchi[73], O. Bienaymé[44], S. Blanco-Cuaresma[15,24,74], T. Boch[44], C. Boeche[13], A. Bombrun[75], R. Borrachero[5], D. Bossini[13], S. Bouquillon[32], G. Bourda[24], A. Bragaglia[27], L. Bramante[29], A. Bressan[76], N. Brouillet[24], T. Brüsemeister[7], E. Brugaletta[51], B. Bucciarelli[26], A. Burlacu[20], D. Busonero[26], A. G. Butkevich[17], R. Buzzi[26], E. Caffau[8], R. Cancelliere[77], G. Cannizzaro[78,63], T. Cantat-Gaudin[13,5], R. Carballo[79], T. Carlucci[32], J. M. Carrasco[5], L. Casamiquela[5], M. Castellani[55], A. Castro-Ginard[5], P. Charlot[24], L. Chemin[80], A. Chiavassa[19], G. Cocozza[27], G. Costigan[12], S. Cowell[2], F. Crifo[8], M. Crosta[26], C. Crowley[75], J. Cuypers[†35], C. Dafonte[53], Y. Damerdji[39,81], A. Dapergolas[33], P. David[34], M. David[82], P. de Laverny[19], F. De Luise[83], R. De March[29], D. de Martino[84], R. de Souza[85], A. de Torres[75], J. Debosscher[38], E. del Pozo[46], M. Delbo[19], A. Delgado[2], H. E. Delgado[60], P. Di Matteo[8], S. Diakite[6], C. Diener[2], E. Distefano[51], C. Dolding[25], P. Drazinos[86], J. Durán[58], B. Edvardsson[48], H. Enke[87], K. Eriksson[48], P. Esquej[88], G. Eynard Bontemps[20], C. Fabre[89], M. Fabrizio[55,11], S. Faigler[90], A. J. Falcão[91], M. Farràs Casas[5], L. Federici[27], G. Fedorets[56], P. Fernique[44], F. Figueras[5], F. Filippi[29], K. Findeisen[8], A. Fonti[29], E. Fraile[88], M. Fraser[2,92], B. Frézouls[20], M. Gai[26], S. Galleti[27], D. Garabato[53], F. García-Sedano[60], A. Garofalo[93,27], N. Garralda[5], A. Gavel[48], P. Gavras[8,33,86], J. Gerssen[87], R. Geyer[17], P. Giacobbe[26], G. Gilmore[2], S. Girona[94], G. Giuffrida[11,55], F. Glass[15], M. Gomes[49], M. Granvik[56,95], A. Gueguen[8,96], A. Guerrier[62], J. Guiraud[20], R. Gutiérrez-Sánchez[23], W. Hofmann[7], G. Holland[2], H. E. Huckle[25], A. Hypki[12,97], V. Icardi[29], K. Janßen[87], G. Jevardat de Fombelle[30],

⋆ Full Table D.3 is only available at the CDS via anonymous ftp to cdsarc.u-strasbg.fr (130.79.128.5) or via http://cdsarc.u-strasbg.fr/viz-bin/qcat?J/A+A/616/A12

⋆⋆ Corresponding author: A. Helmi, e-mail: ahelmi@astro.rug.nl

P. G. Jonker[78,63], Á. L. Juhász[98,99], F. Julbe[5], A. Karampelas[86,100], A. Kewley[2], J. Klar[87], A. Kochoska[101,102], R. Kohley[18], K. Kolenberg[103,38,74], M. Kontizas[86], E. Kontizas[33], S. E. Koposov[2,104], G. Kordopatis[19], Z. Kostrzewa-Rutkowska[78,63], P. Koubsky[105], S. Lambert[32], A. F. Lanza[51], Y. Lasne[62], J.-B. Lavigne[62], Y. Le Fustec[106], C. Le Poncin-Lafitte[32], Y. Lebreton[8,107], S. Leccia[84], N. Leclerc[8], I. Lecoeur-Taibi[30], H. Lenhardt[7], F. Leroux[62], S. Liao[26,108,109], E. Licata[73], H. E. P. Lindstrøm[110,111], T. A. Lister[112], E. Livanou[86], A. Lobel[35], M. López[69], S. Managau[62], R. G. Mann[37], G. Mantelet[7], O. Marchal[8], J. M. Marchant[113], M. Marconi[84], S. Marinoni[55,11], G. Marschalkó[98,114], D. J. Marshall[115], M. Martino[29], G. Marton[98], N. Mary[62], G. Matijevič[87], T. Mazeh[90], S. Messina[51], D. Michalik[3], N. R. Millar[2], D. Molina[5], R. Molinaro[84], L. Molnár[98], P. Montegriffo[27], R. Mor[5], R. Morbidelli[26], T. Morel[39], D. Morris[37], A. F. Mulone[29], T. Muraveva[27], I. Musella[84], G. Nelemans[63,38], L. Nicastro[27], L. Noval[62], W. O'Mullane[18,43], C. Ordénovic[19], D. Ordóñez-Blanco[30], P. Osborne[2], C. Pagani[70], I. Pagano[51], F. Pailler[20], H. Palacin[62], L. Palaversa[2,15], A. Panahi[90], M. Pawlak[116,117], A. M. Piersimoni[83], F.-X. Pineau[44], E. Plachy[98], G. Plum[8], E. Poggio[68,26], E. Poujoulet[118], A. Prša[102], L. Pulone[55], E. Racero[28], S. Ragaini[27], N. Rambaux[34], M. Ramos-Lerate[119], S. Regibo[38], F. Riclet[20], V. Ripepi[84], A. Riva[26], A. Rivard[62], G. Rixon[2], T. Roegiers[120], M. Roelens[15], M. Romero-Gómez[5], N. Rowell[37], F. Royer[8], L. Ruiz-Dern[8], G. Sadowski[21], T. Sagristà Sellés[7], J. Sahlmann[18,121], J. Salgado[122], E. Salguero[40], N. Sanna[10], T. Santana-Ros[97], M. Sarasso[26], H. Savietto[123], M. Schultheis[19], E. Sciacca[51], M. Segol[124], J. C. Segovia[28], D. Ségransan[15], I-C. Shih[8], L. Siltala[56,125], A. F. Silva[49], R. L. Smart[26], K. W. Smith[14], E. Solano[69,126], F. Solitro[29], R. Sordo[13], S. Soria Nieto[5], J. Souchay[32], A. Spagna[26], F. Spoto[19,34], U. Stampa[7], I. A. Steele[113], H. Steidelmüller[17], C. A. Stephenson[23], H. Stoev[127], F. F. Suess[2], J. Surdej[39], L. Szabados[98], E. Szegedi-Elek[98], D. Tapiador[128,129], F. Taris[32], G. Tauran[62], M. B. Taylor[130], R. Teixeira[85], D. Terrett[59], P. Teyssandier[32], W. Thuillot[34], A. Titarenko[19], F. Torra Clotet[131], C. Turon[8], A. Ulla[132], E. Utrilla[46], S. Uzzi[29], M. Vaillant[62], G. Valentini[83], V. Valette[20], A. van Elteren[12], E. Van Hemelryck[35], M. van Leeuwen[2], M. Vaschetto[29], A. Vecchiato[26], Y. Viala[8], D. Vicente[94], S. Vogt[120], C. von Essen[133], H. Voss[5], V. Votruba[105], S. Voutsinas[37], G. Walmsley[20], M. Weiler[5], O. Wertz[134], T. Wevems[2,63], Ł. Wyrzykowski[2,116], A. Yoldas[2], M. Žerjal[101,135], H. Ziaeepour[6], J. Zorec[136], S. Zschocke[17], S. Zucker[137], C. Zurbach[47], T. Zwitter[101]

(Affiliations can be found after the references)

Received 24 January 2018 / Accepted 28 March 2018

ABSTRACT

Aims. The goal of this paper is to demonstrate the outstanding quality of the second data release of the *Gaia* mission and its power for constraining many different aspects of the dynamics of the satellites of the Milky Way. We focus here on determining the proper motions of 75 Galactic globular clusters, nine dwarf spheroidal galaxies, one ultra-faint system, and the Large and Small Magellanic Clouds.

Methods. Using data extracted from the *Gaia* archive, we derived the proper motions and parallaxes for these systems, as well as their uncertainties. We demonstrate that the errors, statistical and systematic, are relatively well understood. We integrated the orbits of these objects in three different Galactic potentials, and characterised their properties. We present the derived proper motions, space velocities, and characteristic orbital parameters in various tables to facilitate their use by the astronomical community.

Results. Our limited and straightforward analyses have allowed us for example to (*i*) determine absolute and very precise proper motions for globular clusters; (*ii*) detect clear rotation signatures in the proper motions of at least five globular clusters; (*iii*) show that the satellites of the Milky Way are all on high-inclination orbits, but that they do not share a single plane of motion; (*iv*) derive a lower limit for the mass of the Milky Way of $9.1^{+6.2}_{-2.6} \times 10^{11}\,M_{\odot}$ based on the assumption that the Leo I dwarf spheroidal is bound; (*v*) derive a rotation curve for the Large Magellanic Cloud based solely on proper motions that is competitive with line-of-sight velocity curves, now using many orders of magnitude more sources; and (*vi*) unveil the dynamical effect of the bar on the motions of stars in the Large Magellanic Cloud.

Conclusions. All these results highlight the incredible power of the *Gaia* astrometric mission, and in particular of its second data release.

Key words. Galaxy: kinematics and dynamics – astrometry – globular clusters: general – galaxies: dwarf – Local Group – Magellanic Clouds

1. Introduction

The possibility of determining for the first time the absolute proper motions of stars in the satellites of the Milky Way opens up a whole new window for understanding their dynamics, origin, and evolution, as well as that of the Milky Way itself. The data presented in the Second *Gaia* Data Release (hereafter DR2, Gaia Collaboration 2018b) allows us to achieve this goal. In this paper we study the proper motions (PM hereafter) of stars in a large sample of globular clusters, in the classical dwarf spheroidal galaxies and one ultra-faint system, and in the Large and Small Magellanic Clouds (LMC and SMC hereafter).

A plethora of interesting science questions can be addressed with this dataset. In this Introduction, we do not aim to be fully comprehensive, but we mention a few topics to set the context, to highlight the power of the unprecedentedly accurate absolute PM measurements, and also to fan curiosity in the community for exploring this outstanding dataset themselves.

Proper motion studies of satellite systems, such as the globular clusters and dwarf galaxies of the Milky Way, have a long history, starting from the use of photographic plates that were sometimes taken with a time baseline longer than 100 years (see Meylan & Heggie 1997 and van Leeuwen et al. 2000 for interesting and thorough historical reviews on the determination of PM of stars in globular clusters). More recently, the space missions HIPPARCOS and the *Hubble* Space Telescope (HST), and of course the *Gaia* mission in its first data release (Gaia Collaboration 2016), have demonstrated the enormous power of space-based astrometry. HIPPARCOS data (Perryman et al. 1997) have been used for many purposes, and in particular, for studying the dynamics of nearby open clusters (e.g. van Leeuwen 1999, 2009), and although HIPPARCOS did not observe stars in globular clusters, it provided an absolute reference frame that was used to derive the orbits of 15 globular clusters from photographic plates, for example (Odenkirchen et al. 1997). On the other hand, the HST has carried out several large (legacy) surveys (e.g. Soto et al. 2017) that have allowed studies of the dynamics of globular clusters and of the Milky Way satellites, and it has even constrained the motions of our largest neighbouring galaxy M31 (Sohn et al. 2012). In all these cases, relative astrometry is done using background quasars and distant galaxies to define a reference frame, and typically, a time baseline of 5–10 yr is used. This has been a highly successful approach, and has, for example, allowed researchers to develop the idea that the Magellanic Clouds may be on their first infall (Kallivayalil et al. 2006b; Besla et al. 2007), to place constraints on the mass of the Milky Way from its most distant satellite Leo I (Boylan-Kolchin et al. 2013), and also to argue in support of the conjecture that dwarf galaxy satellites may lie on a vast polar plane based on the first constraints on their orbits (Pawlowski & Kroupa 2013).

This brief overview gives a flavour of the palette of scientific results that can be derived from accurate PM information of the satellites of the Milky Way. In combination with knowledge of the line-of-sight velocities, PM can be used to derive orbits for these systems. This is interesting for very many reasons, some of which we highlight below.

The orbits of globular clusters can shed light on their formation and evolution, for example, which may have formed in situ and which could be accreted (Searle & Zinn 1978; Mackey & Gilmore 2004; Renaud et al. 2017). Furthermore, knowledge of the orbits helps understanding the effect of tides and the interplay with internal processes, such as evaporation, mass segregation, and two-body relaxation (Djorgovski & Meylan 1994; Baumgardt & Makino 2003). Based on the orbits it is also possible to aid the search for extra-tidal stars and streamers, which are very useful for constraining the gravitational potential of the Milky Way because of the coldness of such streams (Küpper et al. 2015).

In the case of the dwarf galaxy satellites of the Milky Way, knowledge of the orbits also has multiple implications that range from the scale of the formation of the smallest galaxies in the Universe to constraints and challenges to the cosmological model. By determining the orbits of dwarf galaxies, we can establish the effect of the environment on their evolution, including star formation and chemical enrichment histories (Tolstoy et al. 2009), and also the effect of ram pressure stripping, and we can place constraints on the hot gaseous halo of the Milky Way (Nichols & Bland-Hawthorn 2011). The structure of these small galaxies may also have been strongly affected by tidal interactions with the Milky Way, and to quantify the importance of this process, knowledge of the orbits is imperative (Kazantzidis et al. 2011). Furthermore, such knowledge also allows to establish whether there is internal rotation and its amplitude (Battaglia et al. 2008), which is relevant for understanding the formation path of dwarf spheroidal (dSph) galaxies. For the ultra-faint galaxies, whose nature is debated, PM are also useful to identify interlopers, which is particularly important for establishing whether these systems are (on the verge of being) disrupted or embedded in a dark matter halo.

The orbits of the Milky Way satellites (both globular clusters and dwarf galaxies) also provide information on the Milky Way itself, such as its dynamical mass (e.g. Wilkinson & Evans 1999). It is likely that the internal dynamics of the Milky Way have also been affected by the gravitational influence of, in particular, the Sagittarius dwarf (Gómez et al. 2013) and the LMC (Bekki 2012; Gómez et al. 2015), and improved knowledge of the orbits of these objects will allow us to understand what their effect has been. On the other hand, orbits also allow us to gain insight into how a galaxy acquires its satellite population. For example, it has been argued that the satellites lie preferentially on streams (Lynden-Bell & Lynden-Bell 1995), on a thin plane (Kroupa et al. 2005), or that they have fallen in groups (Li & Helmi 2008), of which the LMC/SMC and their recently discovered satellites are direct proof (Bechtol et al. 2015; Koposov et al. 2015). The *Gaia* DR2 data will allow us to establish how real and important these associations are, and also whether the orbits found are consistent with the expectations from the concordance cosmological model.

In this paper we analyse 75 globular clusters in our Galaxy, and we demonstrate that the *Gaia* DR2 PM measurements for these clusters are of outstanding quality, with the formal and systematic uncertainties being effectively negligible. In comparison to previous efforts (e.g. Dinescu et al. 2003; Casetti-Dinescu et al. 2007, 2010, 2013), the errors are reduced by nearly two orders of magnitude. This dramatic improvement will also enable detailed studies of the internal dynamics that could shed light onto how these objects formed and their evolutionary path (Gratton et al. 2012). Some of the questions that might be addressed include whether globular clusters have formed in mini-halos or are fully devoid of dark matter (Ibata et al. 2013). Do they host intermediate mass black holes (Baumgardt 2017)? Are there dynamical differences between the different populations known to be present in many globular clusters (Bellazzini et al. 2012; Bellini et al. 2015; Vesperini et al. 2013)? Has the formation process and evolution for in situ clusters been the same as for those that have been accreted? Have these processes left an imprint on the internal phase-space distribution of their stars? How many clusters show rotation, and what is the link to how they have formed (Hénault-Brunet et al. 2015)? Many of the globular clusters are also being targeted by radial velocity surveys (e.g. Lardo et al. 2015; Kamann et al. 2018), and the combination of *Gaia* DR2 with such datasets will be extremely powerful.

We also study the Magellanic Clouds, the nine classical dSph, and include the ultra-faint dwarf (UFD) Bootes I as an example of what can be achieved with *Gaia* DR2 data. Even though the dwarf galaxies are on average farther away, their mean PMs can be very well determined using *Gaia* DR2, and they are still above the systematic level. Although for many

objects, the uncertainties are comparable to those achievable using the HST, the advantage of having a full view of these galaxies and of the PMs being in an absolute reference frame cannot be over-emphasised. For the dSph, establishing their internal dynamics using this dataset is not yet feasible, however, although perhaps the combination of *Gaia* and the HST will allow to make progress before the end of the *Gaia* mission (as recently demonstrated by Massari et al. 2018). For the Magellanic Clouds, *Gaia* DR2 gives a clearer, more detailed view of the internal dynamics than has ever been possible before, with measured PMs for millions of sources.

The paper is structured as follows. The main part introduces the DR2 data, methods, and analysis, including orbit integrations, and details are given in the appendix. The appendix also contains tables with the measured PM for the objects we studied, as well as a list of the orbital parameters we derived. More specifically, in Sect. 2 of the main paper we present the *Gaia* DR2 data, with emphasis on the astrometry, the selection procedures, and the methods. Section 2.1 focuses on deriving the proper motions of the globular clusters and dSph, and in Sect. 2.2 we describe the procedures that are tailored for the LMC and SMC. We then present the various analyses of the datasets that we have carried out, and which allow us to show the superb quality of the data. Section 3 concentrates on the globular clusters, Sect. 4 on the dSph, and Sect. 5 on the Magellanic Clouds. In Sect. 6 we determine the orbits of the satellites using different Galactic potentials, a showcase of the fantastic possibilities that *Gaia* DR2 offers for studies of the dynamics and origin of the satellites of the Milky Way. In Sect. 7 we discuss our findings, provide an example of the use of DR2 astrometry to find tidal debris, present a summary of what lies beyond a straightforward analysis of the data such as that presented here, and also what will need to wait for later *Gaia* data releases (i.e. the limitations of the *Gaia* DR2 dataset). We present our conclusions in Sect. 8.

2. Data and methods

The data we used are the second *Gaia* data release as described in Gaia Collaboration (2018b). Further details on its validation may be found in Arenou et al. (2018). The procedures to derive the *Gaia* astrometric solution (also known as AGIS) are described in detail in Lindegren et al. (2016, 2018). We recall that the astrometric parameters are absolute in the sense that they do not rely on an external reference frame.

2.1. Globular clusters and dwarf galaxies

The sample of globular clusters analysed in this paper includes half of the whole population of globular clusters in the Milky Way. We focus mostly on the clusters that are located within a distance limit of 12 to 13 kpc to achieve a reasonable compromise on the number of stars with reliable astrometric solutions. It is important to bear in mind that the astrometric solutions for stars in areas of high stellar density, such as the cores of the clusters, are more likely to be disturbed by image blending and onboard image selection. This plays a significant role when observing more distant clusters and affects the fainter stars in particular (see e.g. Pancino et al. 2017). Our selection also takes into account the ability of distinguishing (in PM and parallax space) the cluster stars from those in the field, both as a function of distance from the cluster centre and of magnitude. Furthermore, clusters at low galactic latitude have also generally been avoided to escape confusion with field stars. The top panel of Fig. 1 shows a histogram of the distance distribution for the

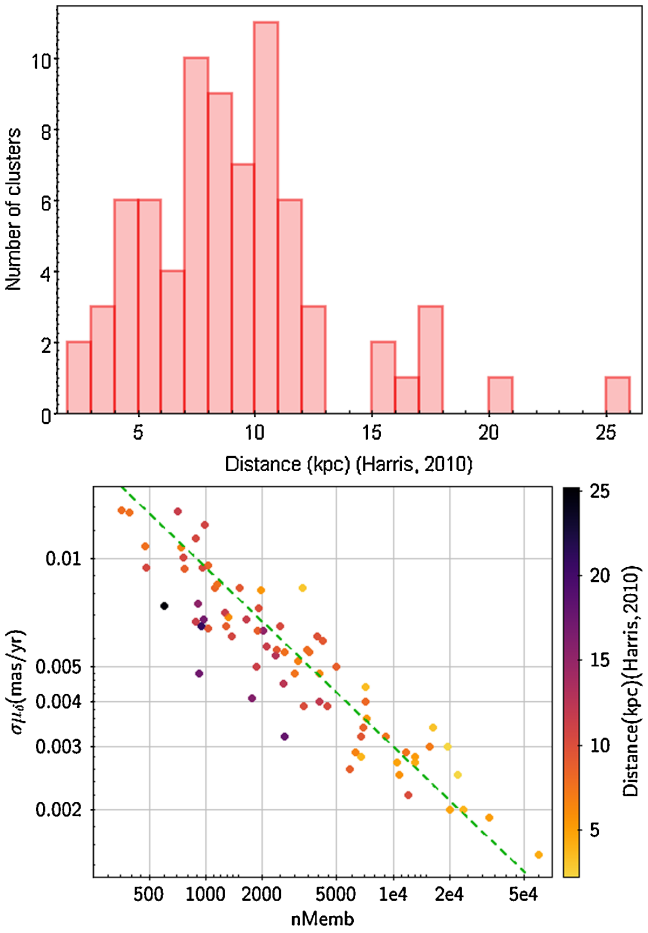

Fig. 1. *Top*: distance distribution of the 75 globular clusters included in the present study. *Bottom*: standard uncertainties on the PM in declination as a function of number of cluster members *nMemb* used in the solution. The diagonal line represents a fit to the relation $\sigma\mu_\delta = a/\sqrt{nMemb}$ where we find $a = 0.3$ [mas/yr]. A similar dependence on the number of members is found for the parallax uncertainty (with $a = 0.15$ [mas]) and for $\sigma\mu_{\alpha*}$ (where $a = 0.25$ [mas/yr]).

75 globular clusters. The bottom panel exemplifies how the standard uncertainties on the cluster PM in declination vary as a function of the number of cluster members used[1].

As Fig. 2 shows, we also studied the classical dSph and one UFD galaxy, Bootes I. UFD galaxies are intrinsically very faint, as their name indicates, and this implies that there are very few stars on the red giant branch (RGB), and depending on the distance to the system, there may be even fewer because of the somewhat bright faint magnitude limit of *Gaia* ($G = 21$). Bootes I is the best UFD case for *Gaia* DR2, because its RGB is relatively well populated (at least in comparison with other UFDs), and it is relatively near (at 60 kpc, Belokurov et al. 2006). These conditions allow us to apply a homogeneous selection and analysis procedure to all the dwarfs in our sample, which we find highly desirable at this point. With external knowledge of radial velocity members, for instance, it might be possible to derive the PM for more UFDs, but the Bootes I case already illustrates the problems to be faced with *Gaia* DR2 data for this type of system.

[1] Note the tendency for more distant clusters to show smaller uncertainties at a fixed number of members. This is driven by the fact that for more distant clusters, only the brighter and less populated part of the luminosity function is effectively sampled, and this implies a lower crowding impact (Pancino et al. 2017).

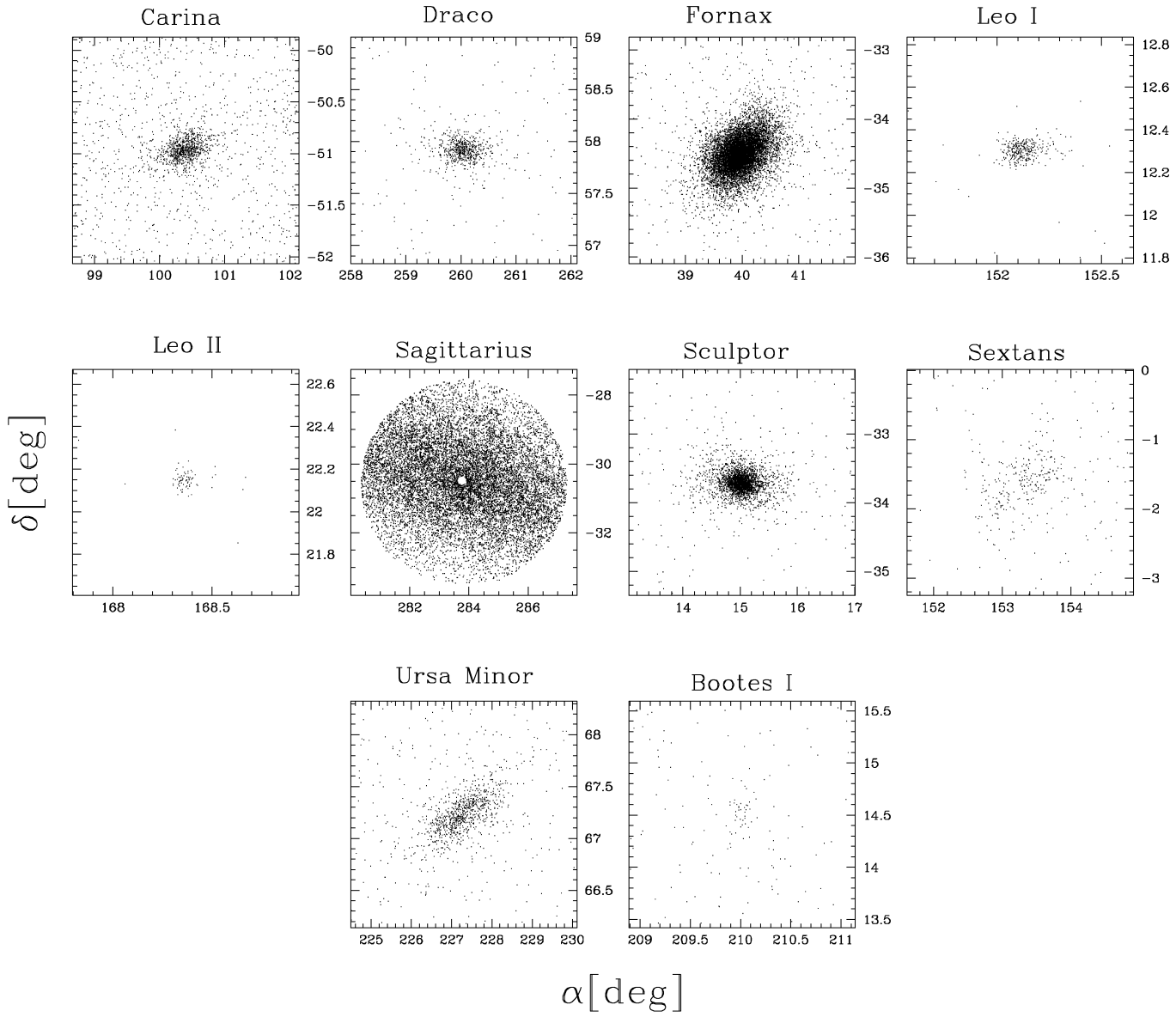

Fig. 2. Field-of-view towards the dSph galaxies (the nine classical and one UFD) in our sample. The stars shown correspond to members according to the photometric selection (on the RGB and BHB) and the astrometric procedure (within 2σ from the mean PM of the object). The striping apparent in Sagittarius and Sextans is driven in part by the scanning law. The hole in the centre of Sagittarius corresponds to the location of the globular cluster NGC 6715 (M54).

The selection procedure, which is described in detail in Appendix A.1, starts with the extraction of data for each object from the GACS archive. The archive provides us with the astrometric parameters, their standard uncertainties and error correlations, the photometric data with standard uncertainties (flux values and fluxes converted into magnitudes), various statistics relating to the astrometric and photometric solutions, and radial velocities where available for our analysis. Depending on the nature of the object analysed, we set different magnitude limits. For the dwarf galaxies, we first considered stars with $G < 21$. For the globular clusters, the limit was generally set at $G = 20$, but in a few cases, we took a brighter value to limit the contamination by field stars. This was necessary for clusters at low galactic latitude in particular.

The *Gaia* sky coverage can locally show strong variations that can affect the selection of members with good astrometric solutions (Gaia Collaboration 2018b; Arenou et al. 2018). In addition, for many of the globular clusters, the central core is often poorly resolved. These conditions are reflected in the standard uncertainties of the derived parameters, but are unlikely to cause a systematic bias in the results. The most strongly affected cluster ω Cen (see Fig. A.6) still shows good astrometric data for very many stars. In the case of the dSph galaxies, the most affected object is Sextans, as can be seen from Fig. 2. The inhomogeneous distribution of sources is related to the number of independent scans in the field of view towards the dwarf. To determine the astrometric parameters reliably, a sufficiently high number of truly independent scans is necessary. This is measured by the parameter `visibility-periods-used`, which has to reach a value greater than 5 for a five-parameter solution for an object (i.e. including the PMs and parallax) to be considered reliable (Lindegren et al. 2018), otherwise, only its position on the sky is determined. There are other instrumental effects that affect the astrometric parameters, and these are discussed elsewhere in the paper and in Lindegren et al. (2018).

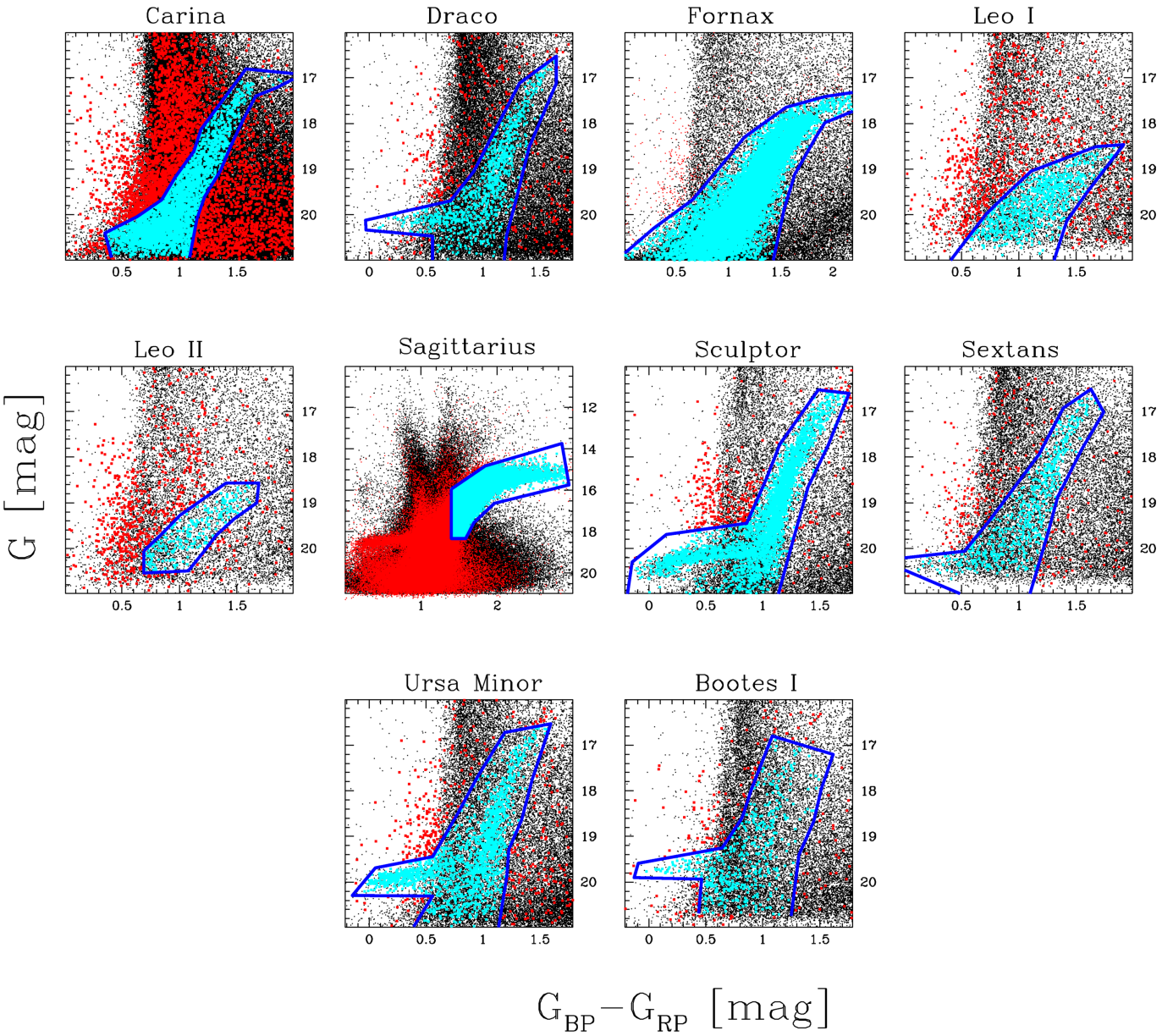

Fig. 3. Colour-magnitude of the stars in the field of view towards the dSph galaxies (the eight classical and one UFD) in our sample. The blue lines mark our (relatively tight) pre-selection of tentative members (on the RGB and BHB) that is fed to the pipeline to derive mean PMs. The coloured points indicate stars within 3σ of our determination of the mean PM of the object. This means that cyan points satisfy both the PM and CMD selections.

The first step in our procedure to derive the motions of the satellites is to focus on an area of the sky, centred on the assumed centre of the object of interest and with an assumed maximum radius. For the dwarf galaxies, these radii were fixed at 2 deg, except for the Sagittarius dwarf, for which we took 3 deg (we also excluded stars within one tidal radius of its nuclear globular cluster M54). For the globular clusters, we interactively explored the data using the TOPCAT software (Taylor 2005), and then made a pre-selection of members based on the concentration of the PMs, followed by a cutoff in parallax, as well as on inspection of the colour-magnitude diagram (for more details, see Appendix A.1).

Because of their low stellar density contrast and the consequently higher number of contaminants (non-member stars) in the field of view, we applied additional selection criteria for the dSph galaxies in order to obtain a more robust estimate of the mean PMs. First, we only considered stars within 1.5× the tidal radius (r_t) of each dwarf (taken from Irwin & Hatzidimitriou 1995; Roderick et al. 2016, for Bootes) except for Sagittarius, where we considered all the stars in the 3 deg radius field of view. Then for all dSph, we also performed a cut in relative parallax error to remove foreground sources, as nearby stars will have relatively good parallaxes, especially in comparison to the stars in the dwarf galaxies. The relative error we used is $0 < \sigma_\varpi/\varpi < 0.5$ (which is equivalent to $\varpi - 2\sigma_\varpi > 0$), and corresponds to removing stars within roughly 5 kpc from the Sun. Finally, we used the distribution of sources in the colour-magnitude diagram (CMD) to isolate the giant branch (RGB and HB), as shown in Fig. 3 with the blue lines. In the case of the Sagittarius dwarf, we used a slightly different selection and focused on the reddest part of the RGB. The reason for this is the very large foreground, which overlaps substantially with the bluer portions of the Sagittarius RGB.

The astrometric solution to derive the PMs and parallaxes for the globular clusters and the dwarf galaxies follows

the procedures described in van Leeuwen (2009); Gaia Collaboration (2017, see also Appendix A.1). A joint solution for the PM and parallax is obtained that takes into account the full error correlation matrix as evaluated for each contributing star:

$$\mathcal{N} = \mathcal{N}_a + \mathcal{N}_v + \mathcal{N}_d. \quad (1)$$

The three main contributions to the noise matrix in Eq. (1) come from the astrometric solution $\mathcal{N}_a$, the estimated contributions from the internal velocity dispersion on the PM dispersion $\mathcal{N}_v$, and the dispersion of the parallaxes from the depth of the cluster $\mathcal{N}_d$, respectively. For the dwarf galaxies, the second and third of these contributions could be ignored, as even the brightest stars in these systems still have standard uncertainties on the astrometric parameters that are relatively large in comparison[2]. Although for most globular clusters the velocity dispersion shows a clear gradient with respect to distance from the cluster centre (see Fig. A.5), we did not take it into account. This would have required a detailed investigation of the actual distribution of the PMs as a function of radial distance, which is beyond the scope of the present paper. The internal velocity dispersion as implemented is an average over the cluster.

The procedure we used to determine the astrometric parameters is iterative and requires a first guess for the parallax and PMs. For the globular clusters, this first guess was obtained using the TOPCAT software (Taylor 2005), as described above. While iterating, several diagnostics are produced, and in particular, we plot the surface density as a function of distance from the centre of the cluster. Such a diagram often shows that the maximum radius initially considered in the data extraction step can be extended farther out (i.e. the background density has not yet been reached). In that case, we retrieved more data from the GACS archive using an increased radius and the latest values found for the PM and parallax. We then repeated the procedure, now with the starting guesses being those given by the latest astrometric solution. This process was repeated until it was clear that the maximum radius had been reached.

The maximum radius for the cluster, that is, the distance from the centre within which we still detect cluster stars (3σ from the mean PM, where σ is the error on the PM derived using Eq. (1)) was compared to the tidal radii r_t extracted from Harris (1996) and its 2010 update (Harris 2010, hereafter Harris10). Figure 4 shows that for the majority of the clusters, this maximum radius is between 1/2 and 2 times the published estimate of the tidal radius. Clusters for which the maximum radius was found to be much smaller than r_t are often affected by a high-density field star population, making the detection of cluster members problematic. We note that r_t has typically been estimated by fitting a King profile to the projected density distribution of stars, and thus does not necessarily nor always reflect the true extent of a cluster (see e.g. Küpper et al. 2010).

In the case of the globular clusters, the contamination by field stars was checked through the dispersion diagrams (see Fig. A.4 for two examples), in which the distribution of PM and parallax was plotted against the standard uncertainties of the measurements, and compared with the expected distributions that include all noise contributions. A contaminating source, such as the SMC for 47 Tuc (NGC 104), shows as an offset over-density in one or more of these charts, and in that case was removed by applying a 3σ filter to the residuals in all three observables, that is, relative PMs and parallax.

[2] We chose to set the intrinsic dispersion to the characteristic 10 km s^{-1} value found for the dwarfs from radial velocity data. However, we have tested different input values and found the results on the mean PM to be robust.

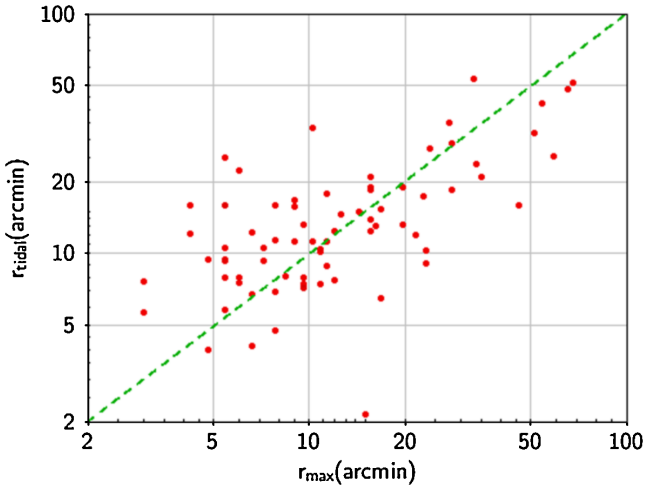

Fig. 4. Comparison between the tidal radii r_t (according to Harris10) of the 75 globular clusters in our sample and the maximum radii at which we have been able to detect cluster members in the present study. The diagonal line represents the one-to-one relation.

We also note that the parallax reference value used for the data extraction was the *Gaia* parallax for the cluster. This can differ from what is considered the best value for the cluster based on the distance from the literature (see Sect. 3 for more details).

In the case of the dwarf galaxies, the iterative procedures are similar, except that further iterations with the GACS archive are not necessary given our choices of initial field sizes. We thus worked only with the data extracted in the first step, as described earlier in this section. We have found, however, that we obtained more reliable mean PM using only stars brighter than a magnitude limit in the range $19.1 < G < 20$. This is the faintest magnitude at which the mean value of the astrometric parameters becomes stable and where the effects of contaminating field stars and the large measurement uncertainties of very faint stars are minimised.

2.2. Magellanic Clouds

The LMC and SMC present a different analytical challenge to the analysis of dwarfs and globular clusters, because they are very extended on the sky and contain two orders of magnitudes more *Gaia* sources than any of the dwarfs or clusters analysed.

To simplify our analysis and ensure that the quoted (and plotted) PMs are relatively easy to interpret in terms of internal velocities, it is particularly helpful to define an orthographic projection of the usual celestial coordinates and PMs:

$$\begin{aligned} x &= \cos\delta \sin(\alpha - \alpha_C) \\ y &= \sin\delta \cos\delta_C - \cos\delta \sin\delta_C \cos(\alpha - \alpha_C) \\ \mu_x &= \mu_{\alpha*} \cos(\alpha - \alpha_C) - \mu_\delta \sin\delta \sin(\alpha - \alpha_C) \\ \mu_y &= \mu_{\alpha*} \sin\delta_C \sin(\alpha - \alpha_C) \\ &\quad + \mu_\delta \left(\cos\delta \cos\delta_C + \sin\delta \sin\delta_C \cos(\alpha - \alpha_C)\right). \end{aligned} \quad (2)$$

The centres of the coordinate systems are chosen to be the dynamical centre of the HI gas for the LMC and SMC, $(\alpha_{C,\mathrm{LMC}}, \delta_{C,\mathrm{LMC}}) = (78.^\circ77, -69.^\circ01)$ and $(\alpha_{C,\mathrm{SMC}}, \delta_{C,\mathrm{SMC}}) = (16.^\circ26, -72.^\circ42)$ (Luks & Rohlfs 1992; Kim et al. 1998;

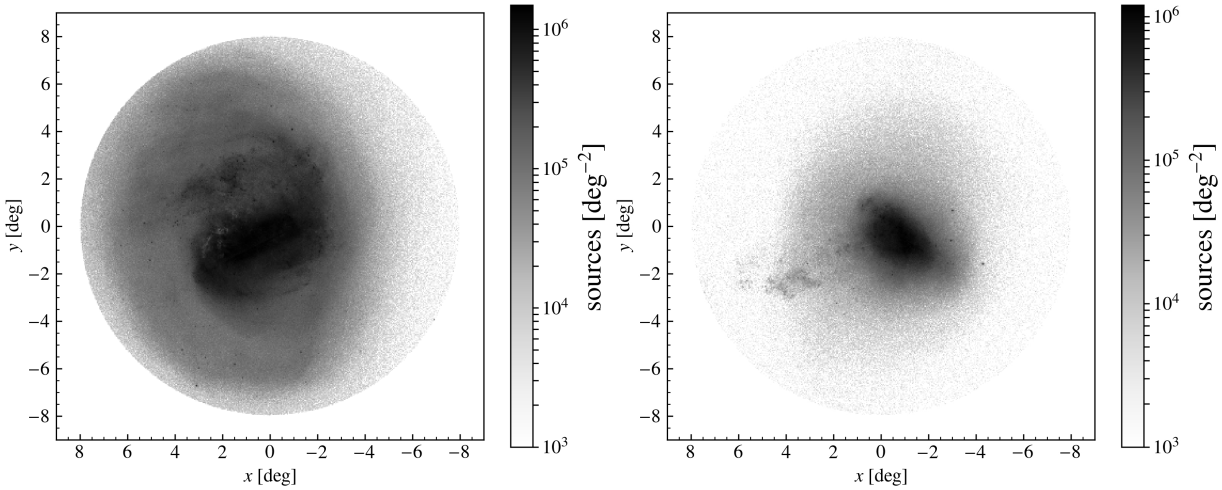

Fig. 5. Density distribution on the sky of the stars selected as members of the LMC (*left*) and SMC (*right*). Positions are shown in the (x, y) coordinates described in the text (Eq. (2)). In all figures that use this coordinate system, the x-axis has been inverted so that it corresponds to the usual inversion of right ascension.

Stanimirović et al. 2004)[3]. Figure 5 shows the density of stars in this x, y-plane for the LMC and SMC, with these centres assumed.

If we approximate each cloud as a thin disc with some bulk motion that rotates about a point with celestial coordinates (α_C, δ_C) with a constant angular velocity ω and no other streaming motion, it can be shown (Appendix B) that these coordinates are, to first order, straightforwardly related to the parameters that describe the position and motion of the disc. These approximations are reasonable towards the centre of the LMC, and serve as a first approximation for the SMC.

It is convenient to define $\boldsymbol{n}$ to be the unit vector normal to the disc (such that rotation is positive about $\boldsymbol{n}$), with $\boldsymbol{z}$ the unit vector from the observer to the reference centre (α_C, δ_C) at the reference epoch. We then have the mutually orthogonal unit vectors in the plane of the disc $\boldsymbol{l} = \boldsymbol{z} \times \boldsymbol{n}/|\boldsymbol{z} \times \boldsymbol{n}|$ and $\boldsymbol{m} = \boldsymbol{n} \times \boldsymbol{l}$. These have the property that $\boldsymbol{l}$ points in the direction of the receding node (the intersection of the disc with the tangent plane of the celestial sphere).

When we define v_x, v_y to be the centre-of-mass motion of the cloud in the x and y directions and v_z to be the same along the line of sight (divided by the distance to the cloud, to put it in the same units) then we have, to first order,

$$\begin{aligned}
\partial\mu_x/\partial x &\approx a v_x - v_z + a l_x m_z \omega \\
\partial\mu_x/\partial y &\approx b v_x - n_z \omega + b l_x m_z \omega \\
\partial\mu_y/\partial x &\approx a v_y + n_z \omega + a l_y m_z \omega \\
\partial\mu_y/\partial y &\approx b v_y - v_z + b l_y m_z \omega
\end{aligned} \tag{3}$$

where with inclination i (the angle between the line-of-sight direction to the cloud centre and the rotation axis of the disc, with $i > 90°$ for retrograde motion)[4], and Ω the position angle of the receding node, measured from $\boldsymbol{y}$ towards $\boldsymbol{x}$, that is, from north towards east, we have the components of $\boldsymbol{l}, \boldsymbol{m}$, and $\boldsymbol{n}$ being

$$\begin{bmatrix} l_x & m_x & n_x \\ l_y & m_y & n_y \\ l_z & m_z & n_z \end{bmatrix} = \begin{bmatrix} \sin\Omega & -\cos i \cos\Omega & \sin i \cos\Omega \\ \cos\Omega & \cos i \sin\Omega & -\sin i \sin\Omega \\ 0 & \sin i & \cos i \end{bmatrix}, \tag{4}$$

and

$$a = \tan i \cos\Omega\,, \quad b = -\tan i \sin\Omega\,. \tag{5}$$

This means that simply by finding a linear fit to the PM as a function of position on the sky, yielding the bulk motion perpendicular to the line of sight, and four gradients, we have four equations for four (in principle) free parameters: v_z, i, Ω, and ω. The first, v_z, produces a perspective contraction (or expansion) as the clouds appear to shrink as they move away from us (or the opposite). The last three describe the orientation and rotation of the disc, which also leave a signature in the PMs.

In practice, neither cloud is flat or expected to have perfectly circular streaming motion. The assumption of a constant angular velocity is approximately valid in the central few degrees of the LMC, but this breaks down at larger radii. Nonetheless, these approximations allow us to draw tentative conclusions about the orientation and velocity curve of the Cloud from these gradients that are simple to measure.

We could take some of the four "free" parameters from other studies, but in practice, we only ever did this for v_z. For the LMC, we took the line-of-sight velocity from van der Marel et al. (2002, $262.2 \pm 3.4\,\mathrm{km\,s^{-1}}$), and the distance from Freedman et al. (2001, $50.1 \pm 2.5\,\mathrm{kpc}$), and for the SMC, we took the line-of-sight velocity from Harris & Zaritsky (2006, $145.6 \pm 0.6\,\mathrm{km\,s^{-1}}$), and the distance from Cioni et al. (2000b, $62.8 \pm 2.4\,\mathrm{kpc}$). This gives us $v_{z,\mathrm{LMC}} = 1.104 \pm 0.057\,\mathrm{mas\,yr^{-1}}$ and $v_{z,\mathrm{SMC}} = 0.489 \pm 0.019\,\mathrm{mas\,yr^{-1}}$.

To determine the PMs of the Clouds, we selected sources using the following procedure:

1. To create a filter, we initially selected stars with $\rho = \sqrt{x^2 + y^2} < \sin r_{\mathrm{sel}}$ ($r_{\mathrm{sel}} = 5°$ for the LMC, $r_{\mathrm{sel}} = 3°$ for the SMC) and $\varpi/\sigma_\varpi < 10$ (to minimise foreground contamination). We also selected only stars with $G < 19$ in

[3] Following van der Marel & Kallivayalil (2014), we have taken the LMC centre to be the average of the centres determined by Kim et al. (1998) and Luks & Rohlfs (1992).

[4] "Retrograde" here means negative spin about the line of sight ($\omega_z < 0$), which means counter-clockwise as seen by the observer. In our notation, the LMC has prograde rotation, that is, positive spin about the line of sight or clockwise as seen by the observer. According to some conventions (e.g. for binary orbits), this would be regarded as retrograde.

this step to ensure that the spread in PM due to uncertainties is small compared to the difference between the PM of the Cloud and of the bulk of the foreground.
2. We determined the median PM of this sample, and preliminarily filtered on PM by removing any source where μ_x or μ_y lies more than four times the robust scatter estimate[5] of that PM component from the median.
3. We determined the covariance matrix of μ_x, μ_y for these stars, $\boldsymbol{\sigma}$, and used this to define a filter on PM, requiring that $\boldsymbol{\mu}^T \boldsymbol{\sigma}^{-1} \boldsymbol{\mu} < 9.21$ to correspond to a 99% confidence region.
4. We applied this filter in PM, along with that in ϖ, to all stars with $G < 20$ within 8 degrees of the assumed centre of LMC or SMC to define our complete sample.

We iterated this procedure twice, first using the expected μ_x, μ_y given the quoted $\mu_\alpha*$, μ_δ. This gave us a median parallax for the stars in the two Clouds: $-19\,\mu$as for the LMC, and $-0.9\,\mu$as for the SMC (compared to the expected values of $\sim 20\,\mu$as and $\sim 16\,\mu$as, respectively). This is consistent with the offset and variation reported in other sections of this paper and in Arenou et al. (2018). We then repeated the procedure using the values of $\mu_\alpha*$, μ_δ implied by the data, conditional on the source parallax taking this median value (taking into account the quoted uncertainties and correlations). This procedure left us with 8 million sources in the LMC and 1.4 million in the SMC.

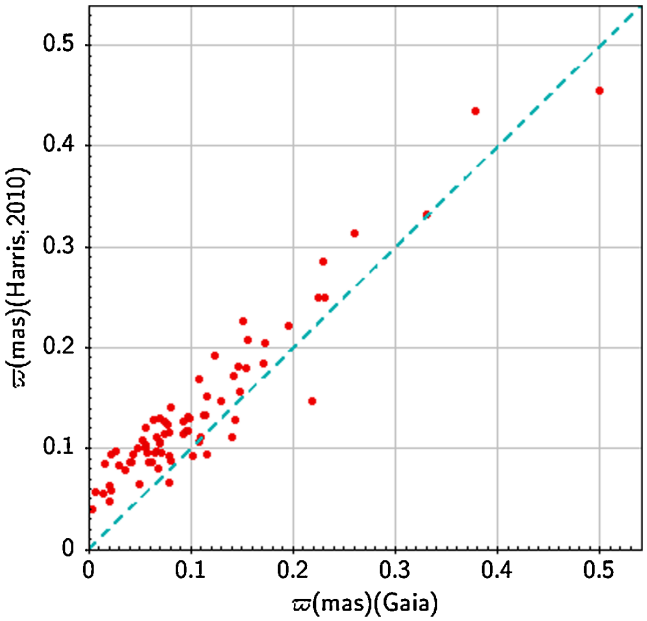

Fig. 6. Comparison between parallaxes as derived from the *Gaia* DR2 data and parallaxes derived from the cluster distances as given in Harris10.

3. Analysis: Globular clusters

As described earlier, we have analysed 75 globular clusters, for which the data are presented in Table C.1. For each cluster we have derived the PM and parallax, and where data were available, the radial velocity.

3.1. First analysis and comparisons

Figure 6 compares the parallaxes derived from the *Gaia* data to those from the cluster distances given in Harris10. There is a systematic difference of –0.029 mas (the *Gaia* parallaxes being smaller), originating largely from the *Gaia* data, and a calibration noise level around that relation of 0.025 mas (Arenou et al. 2018; Lindegren et al. 2018). A small contribution might also come from the values given by Harris10. However, we have made a provisional check on these distance estimates using the *Gaia* photometric data by superimposing the HR diagrams for all the clusters using the distances and reddening values as presented in Harris10 (see Gaia Collaboration 2018a). We found that all the clusters are neatly aligned for the critical elements (mainly the position of the blue horizontal branch). This indicates that, as a group, the distance moduli and colour corrections are confirmed to be in mutual agreement to better than 0.1 magnitude.

The standard uncertainties, which measure the precision rather than the accuracy, of the cluster-parallax determinations are smaller or very much smaller than the overall calibration noise level, as shown in the top panel of Fig. 7. The actual errors on these parallax determinations are therefore dominated by the overall *Gaia* calibration noise and offset in the parallax values. As discussed in depth in Lindegren et al. (2018), these systematic errors are also apparent in the parallax distribution of quasi-stellar objects (QSOs, which reveal the same offset), and as we show in Appendix A.2, also in the parallaxes of stars in the LMC (localised fluctuations) and other dSph, and are due to the basic angle variation and scanning law of *Gaia*. It is therefore expected that their amplitude will be significantly smaller in future *Gaia* data releases. For the time being, and because the parallax uncertainties derived photometrically are smaller, we use the distances as given by Harris10 in the analyses that follow.

The observed PMs are mostly about one to two orders of magnitude larger than the parallaxes, and thus the measurements are very robust and significant (see the bottom panel of Fig. 7). A comparison with a series of studies (Dinescu et al. 1999, 2003; Casetti-Dinescu et al. 2007, 2010, 2013) is shown in Fig. 8, and indicates overall good agreement, and most notably that the errors have been reduced by nearly two orders of magnitude. It remains somewhat uncertain, however, if the same calibration noise level can be assumed for the PMs as for the parallax (but see e.g. Sect. 4.1). Nonetheless, this systematic will be much smaller than the amplitude of the PMs themselves.

Radial velocities as measured by *Gaia* (Cropper et al. 2018) are available for 57 of the 75 clusters, although there were 3 or more cluster stars with measured radial velocities for only 46 clusters. While future *Gaia* data releases will contain radial velocities for more of these sources, this highlights a need for dedicated high-precision spectroscopy of these clusters to properly complement the *Gaia* astrometry. Figure 9 shows a comparison between ground-based (from Harris10) and *Gaia* radial velocity measurements, indicating a good relation for clusters for which enough stars have spectroscopic measurements (darker points). The relation between the number of stars and the standard uncertainty on the mean cluster velocity indicates an average internal velocity dispersion of the order of 4 km s^{-1}. This estimate of the intrinsic velocity dispersions is very similar to what is observed for the PMs.

Figure 10 shows the distribution on the sky of the globular clusters in our sample, where the arrows indicate the direction of motion and the colour-coding reflects the amplitude of the

[5] The robust scatter estimate (RSE) is defined in terms of the 10th and 90th percentile values, P_{10} and P_{90} as $\mathrm{RSE} = C \times (P_{90} - P_{10})$, where $C = \left(2\sqrt{2}\,\mathrm{erf}^{-1}(4/5)\right)^{-1} \approx 0.390152$. For a Gaussian distribution, it is equal to the standard deviation.

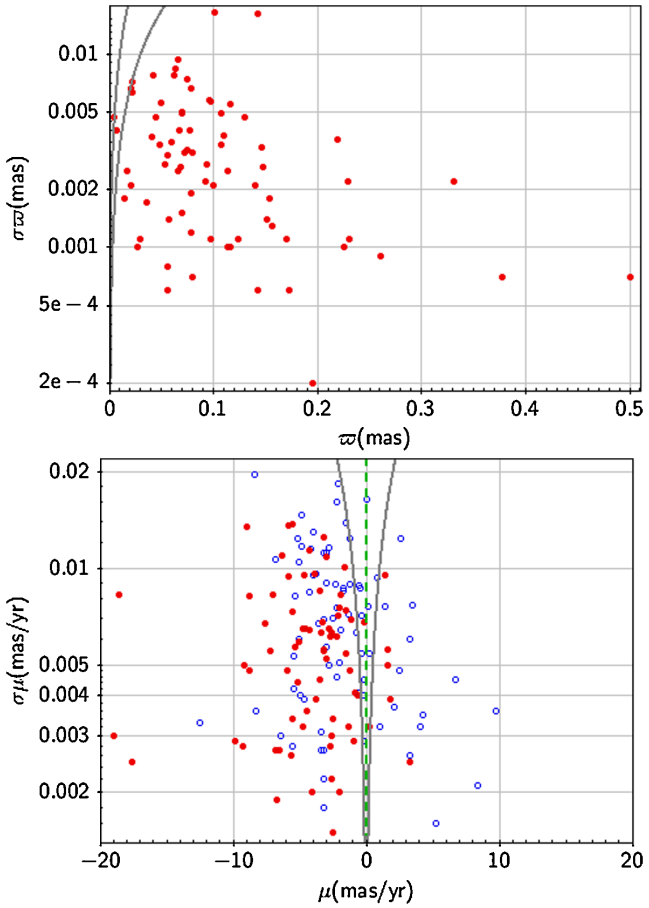

Fig. 7. *Top*: parallax error against the *Gaia* parallax as determined from the *Gaia* data for 75 globular clusters. The black curves are the 1 and 3σ limits. The vertical dashed line corresponds to 3 times our estimate of the systematic error on the parallax. *Bottom*: PM errors against the PMs in right ascension (open circles) and declination (solid circles) for the clusters in our sample. The curves represent the value of the PM for $100\sigma_\mu$. The PM measurement has a significance lower than 10σ only for NGC 6453, for which $\mu_{\alpha*}/\sigma_{\mu_{\alpha*}} \sim 4$.

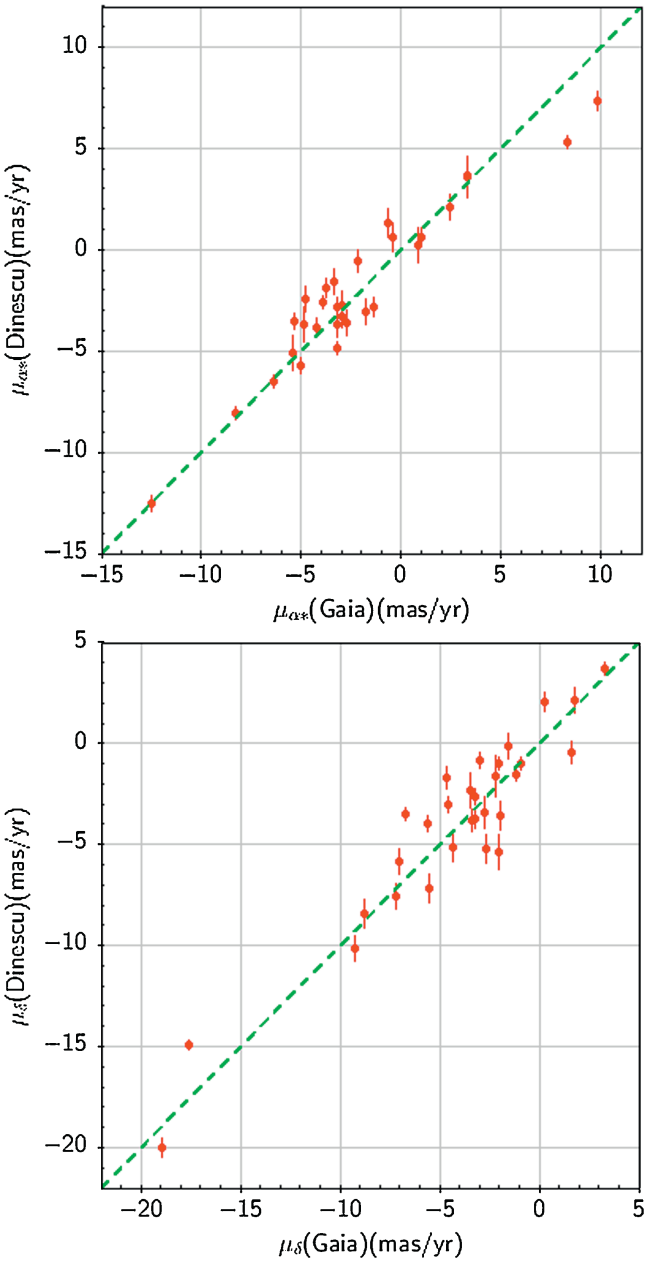

Fig. 8. Comparison of the *Gaia* PMs (in right ascension: *top*, and declination: *bottom*) to measurements reported in Dinescu et al. (1999, 2003); Casetti-Dinescu et al. (2007, 2010, 2013) for 31 globular clusters.

tangential velocities. These were derived using the PMs listed in Table C.1 and the distances from Harris10.

3.2. Further results from the globular cluster astrometric data

The outstanding quality of the *Gaia* DR2 data together with the absolute reference frame (free of expansion and rotation) in which the PMs are presented has also allowed us to clearly detect rotation in 5 of the 75 globular clusters in our sample. For 3 of these clusters (NGC 104, NGC 5139, and NGC 7078), this was already known (Bianchini et al. 2013), but we have also detected rotation in NGC 5904 and NGC 6656 (see e.g. the left panel of Fig. 11). An indication of rotation can also be observed in NGC 5272, NGC 6752, and NGC 6809. Similarly, *Gaia* data allow measuring expansion and contraction in globular clusters. For example, NGC 3201 (Fig. 11, middle) shows very clear perspective contraction, which is due to its very high radial velocity and relatively large parallax. From this we may determine the parallax of this cluster in the same way as this used to be done for the nearby Hyades open cluster (see van Leeuwen 2009, and references therein). The *Gaia* data as presented here for the radial velocity and the PMs thus provide a cluster parallax of 0.221 ± 0.0086 mas, at about 2σ from the value of 0.204 mas given by Harris10. Finally, for NGC 6397, a cluster considered to have been subject to core collapse, we can still see a signal of the expanding halo (Fig. 11, right), clearly different from the expected very weak perspective contraction signal.

Furthermore, we find that our clusters have velocity dispersion profiles that decline with radius (Fig. A.5), and that several clusters show a slight increase in the outskirts, probably as the result of a halo of more loosely bound stars (as evidenced also by their spatial extent, see e.g. Olszewski et al. 2009; Carballo-Bello et al. 2012; Navin et al. 2016; Kuzma et al. 2018). This increase is found at a distance where contamination by field stars should not yet be important.

4. Analysis: Dwarf spheroidal galaxies

The procedures described in Sect. 2.1 allow us to determine the mean PMs of the dSph in our sample. As discussed earlier, we